



Lithological Mapping of Dahab Basin, South Sinai, Egypt, using ASTER Data

ADEL OMRAN, Tübingen, MICHAEL HAHN, Stuttgart, VOLKER HOCHSCHILD, Tübingen, AHMED EL-RAYES & MOHAMED GERIESH, Ismailia, Egypt

Keywords: lithological mapping, band ratio stacking, classification, ASTER, Dahab basin, Sinai, accuracy assessment

Summary: The Advanced Spaceborne Thermal Emission and Reflection Radiometer (ASTER) has gained importance for lithological mapping over the last decade. Its suitability for creating a lithological map of the Dahab basin in south eastern Sinai in Egypt is studied and presented in this paper. For classification and discrimination of different rock types spectral features, in particular band ratios, are used. A new band ratio stacking with a false colour composite created by the ratio stack image (8/5, 4/8, 11/14) is proposed for differentiation between younger granitoids and older granitoids in the southern and central part of the study area. Band ratios 7/6 and 6/4 have turned out to be very suitable for discriminating between cambrian rocks and upper cretaceous rocks in the northern part of study area. Field investigations at different locations of the study area have been carried out to aid in the interpretation and analysis of the ratio stack images. Together with available geological maps the ground truth data is taken into account for selecting training areas and for creating a new map using maximum likelihood classification. An accuracy assessment of the classification result with respect to the regional geological map created by EGSM (1994) and the local area maps of HASSEN et al. (2007) and EL MASRY et al. (2003) indicates overall accuracies between 83% and 94%. An achievement of this study is a lithological map which extends the EGSM map by adding some rock units such as ring-dykes at Wadi Ferani and metasediment, acidic metavolcanics and basic metavolcanics in Wadi Saal and Wadi Ramthy.

Zusammenfassung: *Lithologische Kartierung des Dahab Beckens im Süd-Sinai (Ägypten) mit ASTER-Daten.* Mit dem Sensorsystem ASTER (Advanced Spaceborne Thermal Emission and Reflection Radiometer) werden seit Februar 2000 Daten aufgezeichnet, die einen Beitrag zur detaillierten lithologischen Kartierung leisten können. In diesem Artikel wird die Eignung von ASTER für die Herstellung einer lithologischen Karte des Dahab Beckens im Südosten des Sinai in Ägypten untersucht. Zur Klassifizierung und Diskriminierung verschiedener Gesteinsarten werden aus den 14 ASTER-Bändern ausgewählte spektrale Merkmale (Indexbilder) verwendet, wofür einzelne Bänder zueinander ins Verhältnis gesetzt werden. Die Indexbilder der Bandverhältnisse 6/7 und 4/6 haben sich als sehr geeignet für die Unterscheidung zwischen kambrischen Felsen und oberen Kreidefelsen im nördlichen Teil des Untersuchungsgebietes erwiesen. Mit den zu einem Falschfarbenbild zusammengesetzten Bandverhältnissen (8/5, 4/8, 11/14) wird eine bislang zur lithologischen Kartierung nicht verwendete Kombination vorgeschlagen, die sich zur Differenzierung zwischen den jüngeren und älteren Granitoiden im südlichen und zentralen Teil des Untersuchungsgebietes besonders eignet. Feldbegehungen des Untersuchungsgebietes dienen sowohl dem besseren Verständnis der zu interpretierenden Bilder als auch der stichprobenhaften Erfassung von Ground-Truth-Daten für die Klassifizierung. In einem für die im Dahab Becken vorkommenden Gesteinsarten optimierten Prozess wird eine neue lithologische Karte durch Maximum-Likelihood-Klassifizierung der Indexbilder und eine entsprechende Nachbearbeitung erstellt. Vorhandene geologische Karten (EGSM 1994, HASSEN et al. 2007, EL MASRY et al. 2003) wurden für die Auswahl von Trainingsgebieten, insbesondere auch zur Validierung der erstellten Karte herangezogen. Die Beurteilung der neuen Karte erfolgte anhand von Konfusionsmatrizen, die auf

eine Übereinstimmung mit den vorhandenen Karten zwischen 83% und 94% hindeuten. Die neue Karte erweitert zudem die amtliche geologische

EGSMA-Karte um Ring-Dykes im Wadi Ferani und um Metasedimente sowie um saure und basische Metavulkanite in den Wadis Saal und Ramthy.

1 Introduction

Although Remote Sensing techniques have opened new ways for mapping lithology over the past three decades, the geological maps of the Sinai Peninsula were created based on conventional ground surveys with suitable field observations. A standard procedure was to probe along traverse lines at regular intervals and to plot this point information on a topographic map. The final geological maps then have been created by interpolating the point information and cartographic post processing. By interpolating the sparse point data in a mapping area certain errors are unavoidable and lead to inaccuracies in the map. With remote sensing data the mapping procedures have undergone significant changes. The availability of high resolution multispectral and hyperspectral data has further increased the potential of remote sensing in delineating the lithological contacts and geological structures into greater detail and with better accuracy (DRURY 1987).

A main purpose of the Advanced Spaceborne Thermal Emission and Reflection Radiometer (ASTER) mission is to extend the understanding of local and regional phenomena on the earth surface and its atmosphere. Goals of geologic research using ASTER are summarized by GOMEZ et al. (2005). They put the focus on the "study the geologic phenomena of tectonic surfaces and geologic history through detailed mapping of the Earth topography and geological formation". For the discussion of the importance of the different ASTER wave bands the before mentioned authors refer to early work of KNIPLING (1970), HUNT (1977, 1979), and SALISBURY et al. (1987): "The visible and near infrared (VNIR) wavelength region provides some information for the presence of vegetation, iron oxides (hematite, goethite, jarosite) and rare earth elements. The shortwave infrared (SWIR) wavelength region assesses bearing minerals (clays, phyllosilicates, ...) and the thermal infrared (TIR)

wavelength region permits to distinguish silicates and carbonates".

The study area (Dahab basin, Sinai) is located within an arid climatic belt that crosses northern Africa. Rocks dominate the appearance of the landscape which is sparsely covered by desert vegetation. The goal of this study is to work out details of a classification approach for improving the existing geologic map in the Dahab basin. It further intends to point a way forward for updating the geological maps of the southern Sinai Peninsula as well as for the geologically similar regions in Egypt's eastern desert and in the western part of Saudi Arabia. A second reason for generating the geological map in this study is to provide an updated basis for hydrogeological investigations of the Dahab basin.

Related work

ASTER data have been successfully used in geological mapping since early 2000. In comparison to Landsat TM data, ASTER data has the advantage of combining wide spectral coverage and high spatial resolution in the visible and infrared regions which makes it attractive for geological mapping (e.g. HEWSON et al. 2001, BEDELL 2001). YAMAGUCHI & NAITO (2003) studied spectral index images for lithological mapping. Index images are found by a linear transformation of reflectance values of the five ASTER SWIR bands. The idea of this transformation is to direct the transformation axes to the spectral pattern of the target minerals. The calculated indices are named according to the minerals: alunite, kaolinite, calcite and montmorillonite. An advantage of this approach is that the transformation coefficients are not scene dependent. A simulated ASTER dataset was used to prove the usefulness of the spectral index images.

Some studies used band ratios and the spectral unmixing technique applied to SWIR, TIR and emissivity data of the TIR bands to improve the mapping of the sedimenta-

ry, metasedimentary and volcanic areas. For example, CUDAHY & HEWSON (2002) distinguished some minerals in epithermal, porphyry and skarn groups by using the band ratio technique. ABDEEN et al. (2001) used ASTER band ratios (4/7, 4/1, 2/3*4/3) and (4/7, 3/4, 2/1) for mapping ophiolites, metasediment, volcanoclastics, and granitoid lithologic units of the Allaqi suture in the southeastern part of eastern desert of Egypt.

GAD & KUSKY (2007) recommended to use band ratios (4/7, 4/6, 4/10) for mapping the granite and metamorphic belt of the Wadi Kid area of Sinai and for mapping metamorphic rocks in the Arabian Nubian Shield and other arid areas. REDA et al. (2010) used band ratios (2+4)/3, (5+7)/6, (7+9)/8 to discriminate between different ophiolitic and granitic rocks in the central eastern desert of Egypt. MADANI & EMAM (2009) investigated the band ratio composite (8/5, 5/4, 7/8) to differentiate between alkali granites (younger granitoids), granodiorites and quartz diorite (old granitoids) in the Wadi el-Hudi area, which is located in southeastern desert of Egypt. QARI et al. (2008) utilized the (6/8, 4/8, and 11/14) band ratio image to discriminate the basement rocks in the Arafat area of the Western Arabian Shield, Saudi Arabia, and created a 1:100,000 geological map. Inspired by the work of MADANI & EMAM (2009) as well as QARI et al. (2008) a new band ratio combination (8/5, 4/8, 11/14) is proposed in this study. Details for this new band ratio stacking are given in sections 4 and 5.

WALDHOFF et al. (2008) used Hyperion data and hyperspectral analysis techniques like the minimum noise fraction transformation (MNF), the pixel purity index technique (PPI) and the spectral angle mapper classification (SAM) for geological mapping and compared it with ASTER data classification results. They concluded that the ASTER data allowed a more detailed classification of the surface composition of the study area. This is particularly noteworthy because Hyperion excels by its 220 contiguous spectral bands which cover the spectral range from 400 nm to 2.5 μm at a ground resolution of 30 m. ROWAN & MARS (2003) used in situ measurements of spectral reflectance curves for calibrating the VNIR bands of ASTER. Lithological mapping was carried out by selecting and introducing im-

age spectra of various lithological groups into classification produces. HEWSON et al. (2001) studied a regolith and alteration area in Australia and showed how to improve an existing 1:100,000 geological map with ASTER data. For their investigations they relied on previous surveys using airborne HyMap recordings of visible, shortwave and thermal IR bands and spectral measurements collected in field campaigns. They concluded that their experimental results indicate "that ASTER could discriminate mineral groups not achievable from Landsat TM, though more precise mineral species mapping is not possible".

In the next section background information about the location of the study area and the available ASTER data is given. The geology of the study area is outlined in section 3. In the following two sections 4 and 5 the approach pursued in this research for creating a lithological map of the Dahab basin is presented and processing of the ASTER data using band ratios and supervised classification is discussed in the context of the achieved results. Section 6 summarizes an accuracy assessment of the generated map and presents conclusions of the achievements.

2 Location of the Study Area and ASTER Data

The Dahab basin is considered as one of the major hydrographic basins along the Gulf of Aqaba. The basin is located in the southeastern part of the Sinai Peninsula and is bounded by Latitude 28° 22' 43.4" and 28° 52' 18.5" N and Longitude 33° 55' 46.9" and 34° 31' 28.8" E. It occupies an area of about 2080 km² (Fig. 1, left). It is bordered by the Gulf of Aqaba to the east, Gebel Gidid, Gebel Sheikh El-Arab and Gebel Ferani to the south, Gebel Um Alawi, Gebel Um Loz and Gebel Hamami to the west, and Gebel Bradi and Gebel Gunah to the north (Fig. 1, right). It includes some main wadis in South Sinai as Wadi Nasab, Wadi Ramthy, Wadi Saal, Wadi Zaghraa, and Wadi El Ghaieb.

ASTER data are offered at various processing levels. Level-1A data are reconstructed, unprocessed instrument data at full resolution which consist of the image data, radiometric

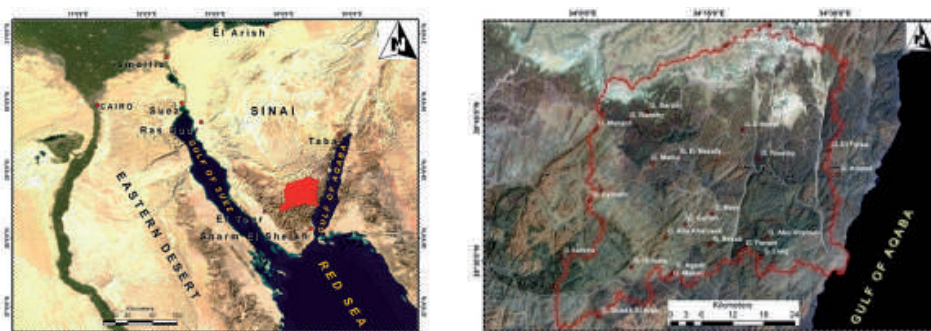


Fig. 1: Left: Location map of Wadi Dahab; right: Basin catchment area.

and geometric coefficients and other auxiliary data without applying the coefficients to the image data to maintain the original data values. The Level-1B data are generated applying these coefficients for radiometric calibration and geometric resampling. The scene used in this research is AST3A1 – 15 bands – 2006 which is a Level-3A data product. This so-called Terrain Correction Image includes Level-1B image data projected in UTM zone 36 (WGS 84) which are orthorectified using a DEM. The scene covers an area of 60 by 60 km² which apart from a small area in south-east encloses the Dahab basin completely.

The proposed procedure for lithological mapping of the study area using ASTER data (sections 4 and 5) mainly relies on the ASTER bands 4, 5, 6, 7, 8, 11 and 14. The spectral ranges of the 30 m resolution SWIR bands are: 1.600–1.700 μm (band 4), 2.145–2.185 μm (band 5), 2.185–2.225 μm (band 6), 2.235–2.285 μm (band 7), and 2.295–2.365 μm (band 8). The TIR bands 11 and 14 record emitted radiation in the wavelength ranges 8.475–8.825 μm and 10.95–11.65 μm , respectively. The spatial resolution of the TIR bands is at 90 m ground pixel size.

3 Geology of the Dahab Basin

The geology of the Dahab basin is discussed by many authors such as HUME (1906), SAID (1962), SOLIMAN (1986), EL SHAFEI et al. (1992), KORA & GENEDI (1995), ZALATA et al. (1997), EL MASRY et al. (2003), and HASSEN et al. (2007). The study area includes many rock

types which can be subdivided according to their age into basement rocks and phanerozoic rocks. In this section the published knowledge on the geology of the basin is summarized with respect to the occurring rock types and its forming minerals.

The reflectance spectra of minerals are well known and catalogued, e.g. in the USGS Digital Spectral Library (CLARK et al. 2007). The fact that rocks are a complex mixture of materials limits the direct utilization of those spectra for remote sensing. The use of the spectra is further lowered by the fairly broad bandwidth and the small number of spectral bands of ASTER. The challenge for the remote sensing approach is to analyse the reflectance of the mineral mix recorded by the ASTER bands. For example, the spectral characteristics of different rocks in the thermal infrared shows a direct dependency on the silica (quartz) contents (KOBAYASHI et al. 2010), so that the ASTER TIR bands will reveal quartz-related information about the rocks. How to reveal the rock specific information and how to exploit it within a classification scheme for lithological mapping will be discussed in sections 4 and 5.

3.1 Basement rocks

The EGSMA map (Fig. 2) shows that basement rocks are the prevalent rocks in the basin area, in particular in the southern and the central part of the basin. Basement rocks can be differentiated into igneous rocks, which cover more than 70% of the study area, and metamorphic rocks which mainly can be found at

Wadi Feirani, Wadi Saal, and some parts of Wadi Zaghraa (Fig. 2). The igneous rock comprises a variety of granitic rocks and younger gabbros. These rocks are intersected with acidic and basic dykes. EL MASRY et al. (2003) indicate the presence of ring-dyke at the Gebel Laig area with younger granitoid rocks.

Granitic rocks

Granitic rocks have wide areal extension at Wadi Nasab, Wadi Ramthy, Wadi Dahab and Wadi El Ghaieb. HASSEN et al. (2004) and EL MASRY et al. (2003) divided the granitic rocks in the study area into late kinematic and past kinematic rocks which is substantially equivalent to older granitoid and younger granitoid rocks. The two groups of older and younger granitoids (Tab. 1) include the EGSMa differentiation of the granitic rocks into monzogranite, alkali granite, granodiorite and quartz diorite.

The mineral composition of younger granitic rocks is quartz and K-feldspar, plagioclase, hornblende and biotite, zircon, apa-

tite, sercite (kaolinite) and opaque minerals. The older granitoids are mainly composed of plagioclase feldspar, K-feldspar, microperthite, hornblende, biotite, and quartz. Zircon, sphene, apatite and opaque minerals are among the accessory components. Weathering of hornblende, biotite and plagioclase leads to form clay mineral (EL MASRY et al. 2003).

Metamorphic rocks

Metamorphic rocks in the study area are distributed along Wadi Saal, Wadi Ramthy and Wadi Zaghraa. SOLIMAN (1986) and HASSEN et al. (2004, 2007) mapped the metamorphic rocks at Wadi Saal and Wadi Zaghraa-Ramthy. They differentiated these rocks into metasediment, basic metavolcanic, acidic metavolcanic and metagabbro. The metamorphic belts are intruded by syn (older) and late (younger) granitoids and gabbroic rocks. Metasedimentary rocks consist mainly of phyllite, metasiltstone, metaconglomerate and volcanogenic sediment, whereas the metavolcanics include a wide variety of metamorphosed rock types such as andesite, dacite and rhyolite associated with minor basaltic bodies (HASSEN et al. 2007).

Tab. 1: Granitic rock types in the Dahab basin area.

Types of granites	Occurring rocks	Forming minerals
older granitoid	granodiorite, quartz diorite, diorite	quartz, plagioclase, hornblende, pyroxene
younger granitoid	alkali granite, monzogranite	quartz, K-feldspar, plagioclase, biotite

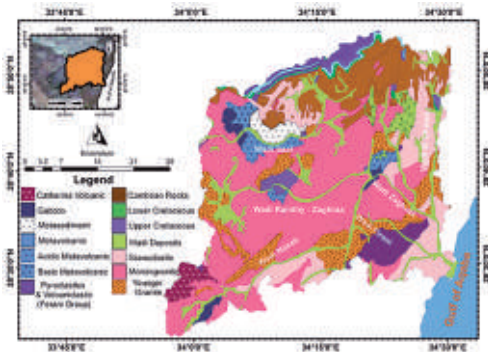


Fig. 2: Geological map of the Dahab basin (adopted from EGSMa 1994).

3.2 Phanerozoic Rocks

Phanerozoic rocks cover the northern part of study area. Their outcrops expose mainly at the scarp of Gebel El Gounah and the northern Part of Wadi El Ghaieb, as well as minor exposures at Wadi Saal and Wadi Genah (Fig. 2). They are represented by a number of geological formations arranged from the oldest to the youngest as: 1) Cambrian rocks consist of laminated sandstone with intercalations of clay and ferruginous bands. They unconformably overlay the basement rocks, are coarse-to-medium-grained, weakly indurated to friable, and include kaolin matrix. 2) Lower cretaceous rocks consisting of grey and violet coloured pebbly and granular sandstone intercalated with kaolin in the upper part and impregnated with iron oxides at the top parts of the sequences. 3) Upper cretaceous rocks have yellow beds of fossiliferous sandstones, dolostones, limestones, marls, and glauconitic

shales with pelecypod moulds, echinoids, and trace fossils of horizontal burrowings. The top of this formation constitutes a thick carbonate sequence of limestone, marl and dolomitic limestone, with thin inter-beds of silty claystone and yellowish-orange, fine-grained sandstone (KORA & GENEDI 1995). Upper cretaceous rocks are mainly exposed at Wadi El Ghaib and Gebel El Gounah Scarp.

Mineralogically, the lower cretaceous rocks are mainly composed of quartz and kaolinite with a minor amount of calcite. This helps to distinguish them from upper cretaceous rocks in which the amount of calcite is high. A high degree of similarity exists in the mineral composition of cambrian rocks and the clastic part of lower cretaceous rocks especially with respect to quartz and kaolinite minerals. But the cambrian rocks are more ferruginated than lower cretaceous rocks, which allows differentiation between them.

4 Methodology

Lithological mapping may be carried out on the computer screen by human interpretation of the images. This is a promising way in particular if the human operator is very experienced. To increase the degree of automation within the mapping process the tools of image classification can be employed. The human operator is still a key factor for the mapping success as he will be involved in selecting proper training areas for supervised classification by taking advantage of existing maps or field visits. The digitized training regions are used to determine statistical parameters for classification. For the well-known maximum likelihood classification these are the mean vectors and covariance matrices for each training class. In maximum likelihood classification, all pixels are evaluated and assigned to the class of highest probability. Maximum likelihood classification of the entire study area in a one step process has been found to be not optimal. The mineral compositions the sedimentary rocks with sandstone of cambrian rocks and of lower cretaceous rocks are similar to the mineral compositions of granite rocks. Therefore, the analysis of the northern part of study area, which includes sedimentary rocks,

is separated from the analysis of the southern part where the basement rocks are forming the main rock component.

The proposed overall process flow for creating a lithological map of the Dahab basin is shown in Fig. 3. The basic idea of this process flow is to use the prior knowledge of the existing EGSMa map to guide classification of the rocks. With this knowledge supervised classification will be specifically applied to the input image data for a certain area. According to the EGSMa map the phanerozoic rocks mainly cover the northern part and basement rocks dominate in the central and southern part of the Dahab basin. For the primary differentiation of phanerozoic rocks and basement rocks our process follows the proposal of ABDEEN et al. (2001). Spatial separation between northern part and central part is done by manual digitization using ASTER band combination 7-3-1.

In each of the two regions band ratio images are used as input for supervised classification of different rock types. For this purpose some band ratios which have been successfully used by other researcher are used. In addition, a new ASTER band ratio stacking (8/5, 4/8, 11/14) is introduced. The training areas for the maximum likelihood classification are selected on the basis of existing geologic maps together with supporting field visits. As a part of this study, field visits at 23 locations of the study area have been undertaken. However, the idea to use the field mapped data as reference was rejected because of the small sample size. Therefore, the geologic maps are further used as references for evaluating the accuracy of the classification result.

Band ratioing has been widely used for lithological mapping due to its proven ability to produce distinct grey tones of imaged materials in certain ratios. A band ratio is created by dividing the digital number (DN) of one band by the corresponding DN of another band for each pixel (DRURY 1987). The majority of fractional values are between zero and two or three. Thus, for visibility reasons the ratios are often rescaled to produce ratio images with higher contrast. Another well-known effect of ratioing is the reduction of the impact of shadow in the ratio images. Which band ratio is particularly suitable for enhancing a

certain rock type or mineral depends on the dominance of the mineral in the reflected data. Spectral signatures give useful hints to decide about the bands used for ratioing. Combinations of three band ratio images can be visualized as colour composites. Features or minerals show up in distinct colours in these stacked ratio images. The question of which band ratios or band ratio stackings enhances the visibility of a particular rock type is analysed and discussed extensively in the next section.

The processing flow (Fig. 3) points out the different band ratio images used for maximum likelihood classification. In the northern part of the basin the mapped classes are cambrian rocks, upper cretaceous and lower cretaceous rocks, granodiorite and wadi deposits. In the central and southern part of the basin there are the metamorphic rocks with metavolcanic, basic metavolcanic, acidic metavolcanic, meta-sediment, phyllite and metagabbro. Wadi deposits are also taken into account in particular for comparison reasons with the reference map. For the igneous rocks as the other major group in the central and southern part of the study area the rock type classes granodiorite, alkali granite, monzogranite are mapped by image classification. Ring dykes are visually recognizable in the image. Supported by field visits they have been digitized interactively. In classifying this group of igneous rocks the metamorphic Feirani metavolcaniclastic rocks are added for comparison reasons with the reference map.

A post classification smoothing of the classification results is carried out by majority filtering and with the suppression of very small areas. The results of the lithological mapping process are the data found by vectorisation of the post processed classification maps.

The classification accuracy assessment is the last step in the overall processing flow (Fig. 3). For assessing the derived map quantitatively the error matrix method is used which compares the classification map against a reference. Ideally a representative sample of field mapped ground truth data are used as reference data. Due to the lack of suitable ground truth data the existing geologic maps are used. The EGSMA map is used as reference in the northern part of the basin. The more detailed map of HASSEN et al. (2007) is used as refer-

ence in the areas of Wadi Saal and the Wadis Zaghraa and Ramthy. The map of EL MASRY (2003) is taken as reference in the areas of Wadi Nasab, Wadi El Ghaieb und Wadi Feirani. The limitations of this accuracy analysis are obvious; the error matrix provides information about how well the classification map and the existing maps coincide.

5 ASTER Data Analysis, Classification Results and Discussion

The usefulness of Landsat ETM band combination 7-4-2 for geological mapping in arid regions and the far-reaching consistency of this band combination to ASTER band combination 7-3-1 are pointed out by ABDEEN et al. (2001). Fig. 4 left shows ASTER band combination 7-3-1 in which the metamorphic rocks appear in greenish and reddish colour, the granitic rocks as light yellow to light brown, the sedimentary rocks as white colour, and the wadi deposits as light grey colour. A manual mapping result of the wadi deposits is shown in Fig. 4 right. This vector layer of the wadi deposits will be used as overlay in other figures to simplify visual orientation.

5.1 Central and Southern Part of the Dahab Basin: Igneous Rocks

A new band ratio stacking with the ratio images (8/5, 4/8, 11/14) is used for differentiation between younger granitoids and older granitoids in the central and southern part of the study area. For a better understanding of this stacking the band ratio images are discussed in the context of the spectral signature of the dominant minerals.

Band ratio 4/8: Alkali granite appears dark, monzogranite grey, older granitoids show light grey to bright colour (Fig. 5A). The light colour of older granitoids is due to alteration products of hornblende and plagioclase into chlorite and clay minerals, whereas the presence of biotite and K-feldspar minerals in alkali granites (EL MASRY et al. 2003) produces a dark colour in band ratio 4/8. The dark col-

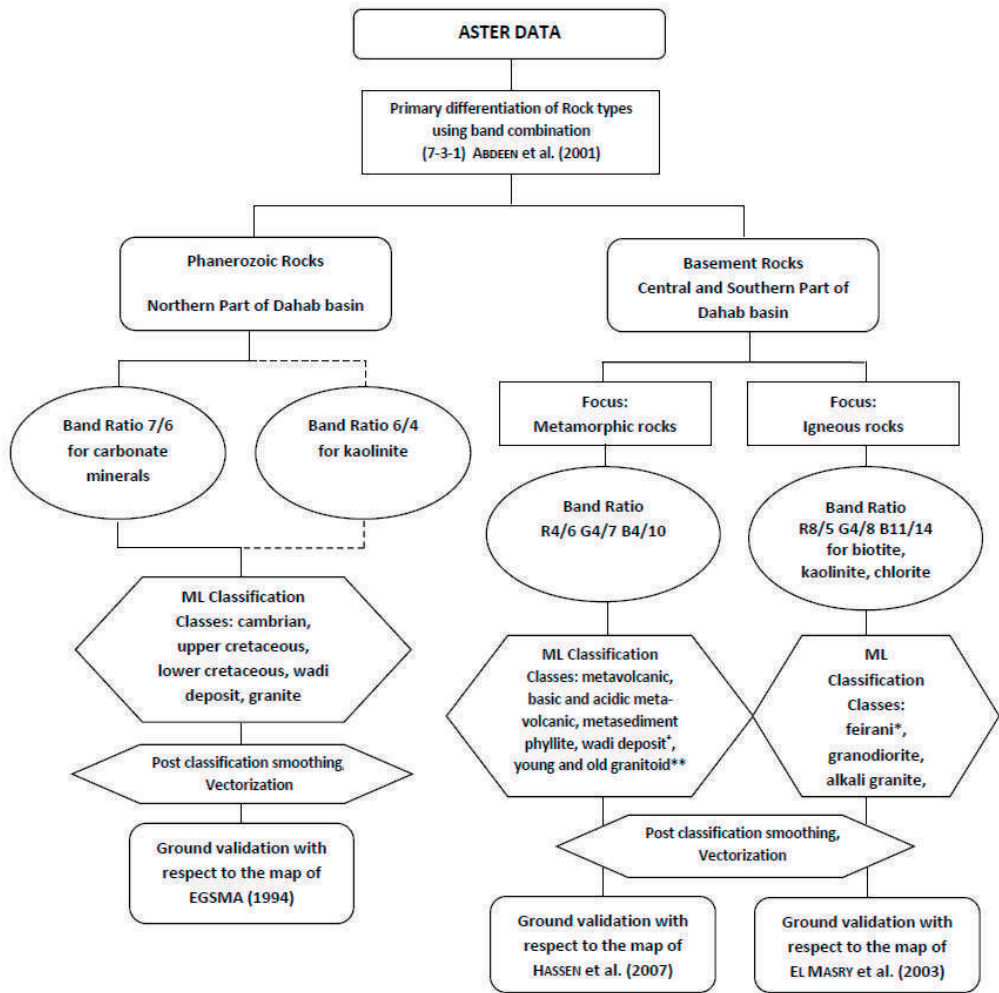


Fig. 3: Overall process flow for lithological mapping of the Dahab basin area (* is a metamorphic rock, ** is an igneous rock, + are not introduced into ML classification).

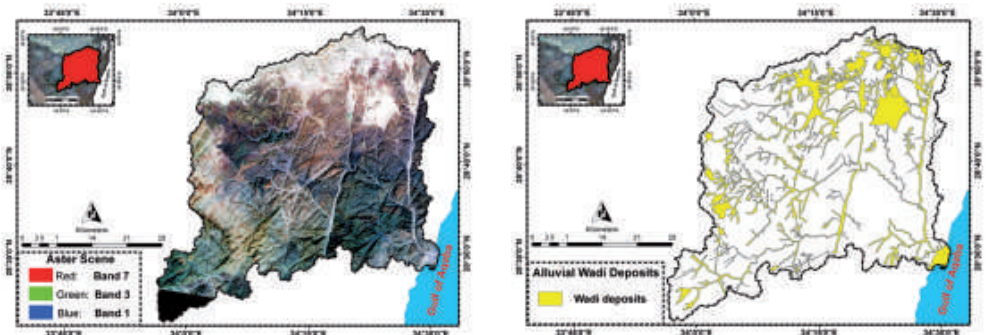


Fig. 4: Left: band combination 7-3-1 of Dahab basin area; right: map of the wadi deposits.

our is a consequence of the lower reflectance in band 4 (Figs. 5 B and C).

Band ratio 8/5: Younger granitoids appear as light grey and older granitoids as grey colour (Fig. 6A). In band ratio image 8/5, Feirani metavolcaniclastic rocks show dark grey colour. This is due to the presence of biotite and K-feldspar in addition to the alteration products of hornblende and plagioclase into clay minerals. Rocks rich in feldspar commonly weather to kaolinite. Fig. 6B shows an absorption feature of kaolinite near band 5 thus the high 8/5 band ratio values indicate younger granitoids. On the other hand, dark grey and grey colours of old granitoids and metamorphic rocks are due to the absorption property of chlorite (Fig. 5C), which leads to low 8/5 band ratio values.

Band ratio 11/14: Younger granitoids appear as dark colour, older granitoids show light grey to bright colour (Fig. 7). The dark colour of younger granitoids may be interpreted by their high ability to reflect the sun radiation on their light coloured surfaces, and hence they represent cooler surfaces which appear dark in the band image. In contrast, older granitoids

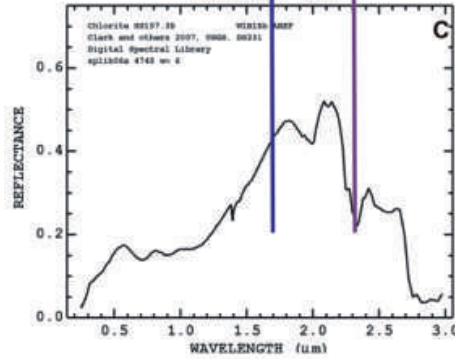
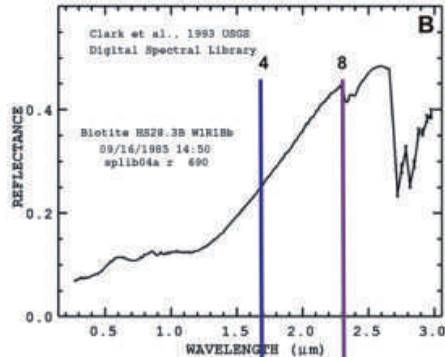
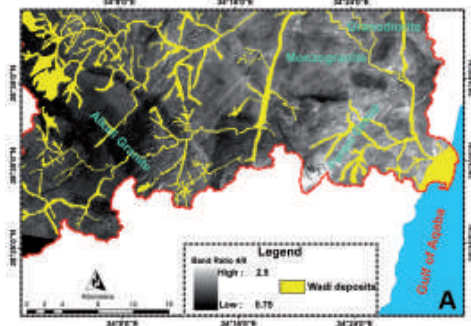


Fig. 5: A: band ratio 4/8 image; B: spectral signature of biotite; C: spectral signature of chlorite (CLARK et al. 2007).

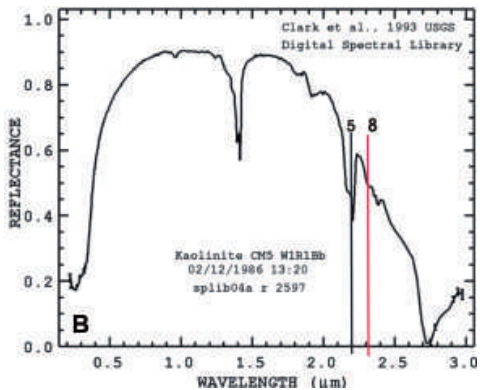
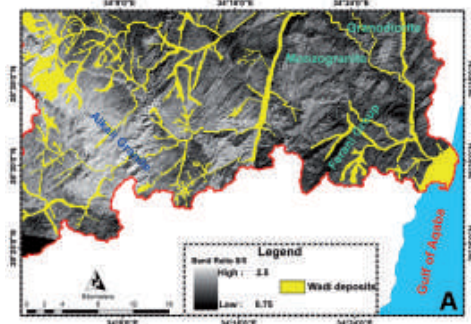


Fig. 6: A: band ratio 8/5 image; B: spectral signature of kaolinite (CLARK et al. 2007).

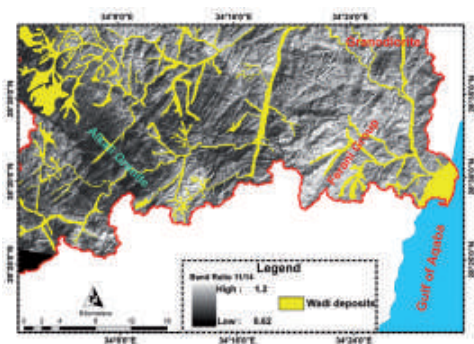
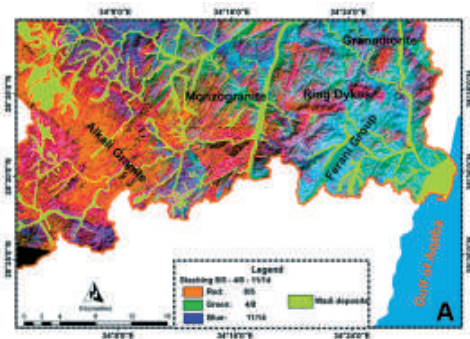


Fig. 7: Band ratio 11/14 image.

absorb more sun radiation and get warmer than other rock types and hence appear brighter in the band image.

In experiments with different band ratio stackings, we found that the colour composite (8/5, 4/8, 11/14) reveals subtle differences between the younger and older granitoids. Fig. 8A shows alkali granites that appear in red colour, monzogranites and acidic volcanic which show up in pink colour. The Feirani group appears as light green whereas older granitoid looks green and purple. The visual comparison of this new stacking with the ratio stack image (8/5, 5/4, 7/8) used by MEDANI & EMAM (2009) in the El Hudi area of southeastern desert in Egypt shows its strength with respect to the discrimination of younger granitoids. Alkali granite and monzogranite rocks are much better discriminated in the new stacking. But with respect to older granitoids (granodiorite and Qz diorite) the MEDANI & EMAM (2009) stacking seems to be a bit more favourable.



The colour composite of the single band ratios is used for defining the training areas of the four rock classes alkali granites, monzogranites, Feirani metavolcaniclastic, and old granitoids. For each class several (minimum 4) training areas are selected to get representative samples. In Fig. 10B the maximum likelihood classification result of the four rock classes is shown together with the wadi deposit layer. Alkali granites are colorized in red, monzogranites in pink, Feirani metavolcaniclastic in light green, old granitoids in dark green and wadi deposits in yellow.

For the accuracy investigation of the classification result the geologic map of EL MASRY et al. (2003) is used as reference. This local area map was generated based on detailed field work and covers the Gebel Feirani area. Fig. 2 shows the location of the Gebel Feirani area at the downstream part of the Dahab basin. In addition to alkali granites, monzogranites, and Feirani metavolcaniclastic, the EL MASRY map includes granodiorite, Qz-diorite, and tonalite. The latter two cannot be distinguished from granodiorite by image classification. Therefore, the prevalent granodiorite is introduced as a class on its own. Ring-dyke is interactively mapped because it is visually recognizable by its dyke-like body (Fig. 8). It has the same composition as alkali granites thus belongs to this class in the classification map.

The quantitative comparison between the results of the classification map and the reference map is summarized by the error matrix in Tab. 2. Reference data are selected from the reference map for the raster locations defined by the classification map. The procedure for

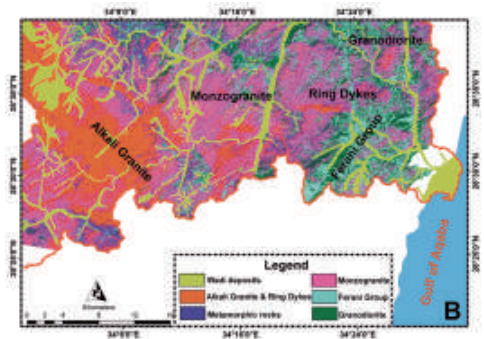


Fig. 8: A: stacked band ratio image (8/5, 4/8, 11/14); B: ML Classification using the stacked band ratio image (8/5, 4/8, 11/14).

Tab. 2: Accuracy evaluation of the classification map for igneous rock types.

		Class types from the reference map					Total	User's Accuracy
		Ferani	Grano	Alkali	Monzo			
Class types of the classification map	Pixels							
	Feirani	393	47	0	5	445	88%	
	Granodiorite	81	392	8	3	484	81%	
	Alkali Granite	0	5	775	18	798	97%	
	Monzogranite	1	13	177	413	604	68%	
Total		475	457	960	439	2330		
Producer's Accuracy		83%	86%	81%	94%		85%	

selecting samples in each category follows the stratified random sampling strategy. For each class in the classification map 4 to 5 samples are taken as reference data.

The results indicate an overall accuracy of 85%. Apart from the user's accuracy of 68% for monzogranite the user's and producer's accuracies of the other classes are all above 80%. The interfering contacts between monzogranite and alkali granite lead to a fairly high misclassification of monzogranite with the consequence of a low user's accuracy for this class. Similar is the situation for the Ferani metavolcanics and the granodiorite but with less significant consequences for the user's accuracy.

5.2 Metamorphic Rocks

The band ratio stacking (4/6, 4/7, 4/10) shows the metavolcanic (metatuffa) rocks in greenish yellow and the basic metavolcanic rocks in

reddish brown colour. The acidic metavolcanic rocks show up by light violet colours, the metasediment phyllite rocks in light green, the younger granitoid rocks have dark blue colour and the light blue colour refers to old granitoid rocks (Figs. 9 A and B).

Training areas have been defined in the colour composite (4/6, 4/7, 4/10) by following the same procedure described already in section 5.1. The classification is carried out for seven classes of rock units. Fig. 10 shows the classification results for Wadi Saal (Fig. 10A) and Wadi Ramthy (Fig. 10B). Metavolcanics is colourized in blue, basic metavolcanics in purple, acidic metavolcanics in light green, metasediments (phyllite) in dark green, younger granitoid in red, older granitoid in pink and meta-sedimentary rocks (in Wadi Ramthy only) in dark green. Wadi deposits have been also introduced into classification and show up in yellow in the classification map.

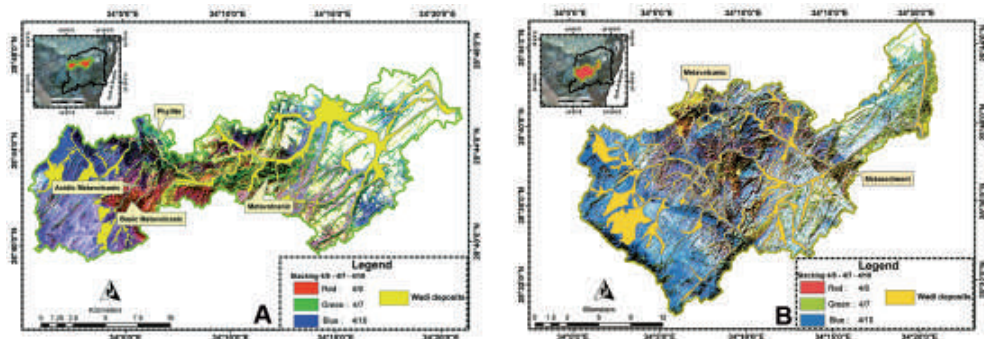


Fig. 9: Stacked band ratio (4/6, 4/7, 4/10) images; A: Wadi Saal area; B: Wadi Ramthy area.

For the accuracy investigation the classification maps are compared to the geologic map created by HASEN et al. (2007) based on field observations. This geologic map covers the areas of the Wadis Saal, Zaghraa and Ramthy. The error matrix found by stratified random sampling is listed in Tab. 3.

The overall accuracy of 83% confirms the good matching between the classification map and HASEN's reference map for both wadis. The error matrix (Tab. 3) has quite some similarity to the error matrix found for the classi-

fication of the igneous rocks (Tab. 2). The producer's accuracy is fairly high between 79% and 96% for all classes. The user's accuracy of 66% for metasedimentary rocks suffers from misclassification with metavolcanics and basic metavolcanics rocks. The small outcrops of acidic metavolcanics, metasediments, wadi deposits, and older granitoids produce a lot of uncertainty with respect to the other classes which results in user's accuracies between 66% and 76% for these classes.

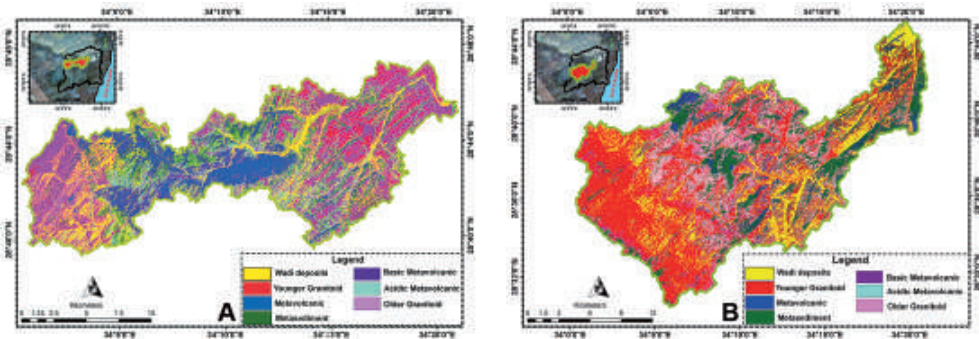


Fig. 10: ML classification of stacked band ratio (4/7, 4/6, 4/10) images; A: Wadi Saal; B: Wadi Ramthy.

Tab. 3: Accuracy evaluation of the classification map for metamorphic rock types.

		Class types from reference source							Total	User's Accuracy
		met_vol	met_ba	met_ac	met_sed	wd	young	old		
Class types of the classification map	Pixels									
	Metavolcanic	281	23	1	0	0	0	1	306	92%
	Basic metavolcanic	49	181	0	2	3	0	0	235	77%
	Acidic metavolcanic	3	11	56	0	1	3	0	74	76%
	Metasediment	8	11	1	41	1	0	0	62	66%
	Wadi deposits	5	2	1	3	28	1	0	40	70%
	Younger granitoid	0	0	4	0	0	73	0	77	95%
Older granitoid	0	0	2	0	0	5	22	29	76%	
Total		346	228	65	46	33	82	23	823	
Producer's Accuracy		81%	79%	86%	89%	85%	89%	96%		83%

5.3 Northern Part of the Dahab Basin: Sedimentary Rocks

Band ratio 7/6 can be used to differentiate sedimentary rocks with respect to carbonate minerals, in particular calcite and aragonite which are the main components of limestone (upper cretaceous) rocks. The absorption features of calcite near band 7 (Fig. 11B) together with its high reflectance in band 7 produces the dark appearance of the cretaceous rocks in Fig. 11A. The cambrian rocks appear as bright colour, whereas the granites appear as darker grey tone.

Alternatively band ratio 6/4 can be used to discriminate between different classes of sedimentary rocks. Quartz with kaolin (altered to clay) together with iron oxide are the main minerals of cambrian rocks which lead to dark colours in this band ratio because of the ab-

sorption feature of kaolinite near band 6 and the high reflectance in band 4. Upper cretaceous rocks show up in grey and granites appear in bright tones in band ratio 6/4 (Fig. 12). A visual comparison of the 7/6 versus the 6/4 band ratio indicates that the discriminative efficiency of 7/6 ratio is higher than that of the 6/4 ratio. Therefore, the analysis focused in analysing band ratio 7/6. A joint use of both bands would have been possible but was not pursued in this analysis.

Supervised classification including post classification smoothing and vectorization is carried out by taking band ratio 7/6 as input image. In the classification map, upper cretaceous rocks is colourized in red and lower cretaceous rocks in light green. For granites violet and for cambrian rocks blue is used. Wadi deposits appear yellow in the classification map (Fig. 13).

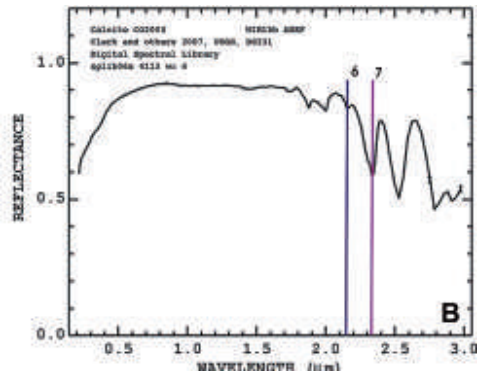
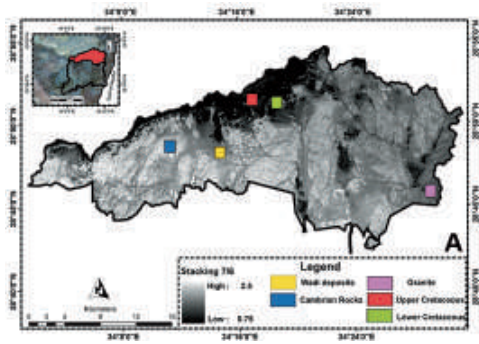


Fig. 11: A: band ratio 7/6 image of the northern part of Dahab basin area; B: spectral signature of calcite (CLARK et al. 2007).

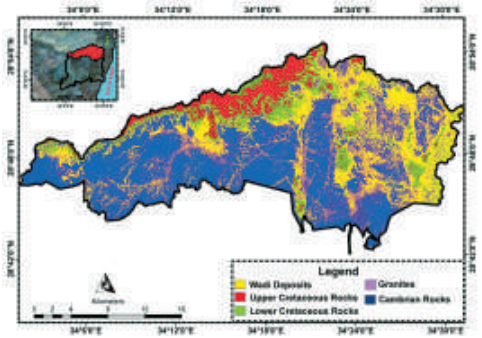
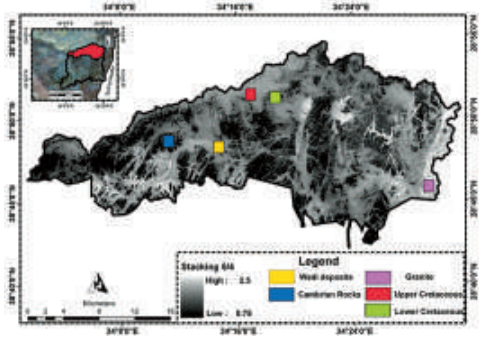


Fig. 12: Band ratio 6/4 image of the northern part of the Dahab basin.

Fig. 13: Supervised classification of band ratio 7/6 image of the northern part of Dahab basin.

Tab. 4: Accuracy evaluation of the classification map for phanerozoic rock types.

		Class types from reference source						User's Accuracy
Class types of the classification map	Pixels	Camb.	Up. Cret.	wd	Low. Cret.	Gran.	Total	
	Cambrian rocks	191	0	0	0	23	214	89%
	Upper Cretaceous	0	97	0	6	0	103	94%
	Wadi deposits	0	0	994	2	13	1009	99%
	Lower Cretaceous	0	12	1	131	3	147	89%
	Granites	1	0	36	2	111	150	74%
	Total	192	109	1031	141	150	1623	
Producer's Accuracy		99%	89%	96%	93%	74%		94%

For the accuracy investigation the geological map provided by EGSM (1994) is used as a reference. The overall accuracy is quite high (94%, Tab. 4). User's and producer's accuracies of 89% to 99% indicate a high agreement of the classification map and the reference. The only exception are the granitic rocks with a user's and a producer's accuracy of 74%. Granitic rocks and alluvial wadi deposits are in contact with each other which is probably the main reason for this lower accuracy.

The final geological map of the Dahab basin created according to the proposed process flow (Fig. 3) is shown in Fig. 14. It comprises 19 classes of phanerozoic, metamorphic and igneous rocks. Apart from the ring dykes all other classes have been created by supervised image classification followed by post classification smoothing and vectorization of the raster data.

6 Conclusion

The investigations on the suitability of ASTER data for lithological mapping have led to the development of an overall processing strategy for mapping granitic rocks, metamorphic rocks and sedimentary rock in Wadi Dahab basin. The goal to develop a classification based approach in which only minor interactive digitization is included is fully achieved. Interactive digitization was used to separate the northern and the central and southern part of the basin as well as for the mapping of the

ring dykes. The study shows the suitability of maximum likelihood classification taking various band ratios and band ratio stackings into account. Through classification different types of granitoid rocks (monzogranites, alkali granites, granodiorites), metamorphic rocks (metasediments and metavolcanics) and phanerozoic rocks (Cambrian, lower Cretaceous, upper Cretaceous rocks and loose wadi deposits) have been differentiated. For checking the quality of the classification map an accuracy assessment is carried out. For this purpose an error matrix is determined which compares the classification map with respect to existing geologic maps.

As a part of the development a new band ratio stacking (8/5R, 4/8G and 11/14B) is proposed for differentiation of younger granitoids (monzogranites and alkali granites) and older granitoids (granodiorite) in the Dahab area. Alkali granite and monzogranite rocks are very well discriminated by the new stacking. With respect to older granitoids (granodiorite, Qz diorite and tonalite) MEDANI & EMAM (2009) stacking seems to be still more favourable. For the discrimination of different metamorphic rock types our procedure follows the proposal of GAD & KUSKY (2007) by applying the band ratio stacking (4/6R, 4/7G and 4/10B). The phanerozoic rocks in the northern part of study are differentiated using the (7/6) band ratio.

The accuracy investigations of the classification results are carried out with respect to the geological reference maps published by

HASSEN et al. (2004), EL MASRY et al. (2003) and EGSMA (1994). The calculated error matrices indicate overall accuracies between 83% and 94%. Altogether this underlines that the created lithological map fits reasonably well to the existing maps which have been mainly created by field work. The created lithological map adds some rock units to the general geological map of EGSMA. Added are ring-dykes at Wadi El Ghaieb, acidic metavolcanics, basic metavolcanics and metasediments at the Wadis Saal, Zaghraa and Ramthy and metasediments at Wadi Ramthy. Alluvial wadi deposits are also included in the final lithological map as shown in Fig. 14.

References

ABDEEN, M.M., ALLISON, T.K., ABDELSALAM, M.G. & STERN, R.J., 2001: Application of ASTER band-ratio images for geological mapping in arid regions; the Neoproterozoic Allaqi Suture, Egypt. – *Geological Society of America* **3** (3): 289.

BEDELL, R.L., 2001: Geological mapping with ASTER satellite: new global satellite data that is a significant leap in remote sensing geologic and alteration mapping. – *Special Publication Geological Society of Nevada* **33**: 329–334.

CLARK, R.N., SWAYZE, G.A., WISE, R., LIVO, K.E., HOEFEN, T.M., KOKALY, R.F. & SUTLEY, S.J.,

2007: USGS Digital Spectral Library splib06a. – U.S. Geological Survey, Data Series **231**.

CUDAHY, T. & HEWSON, R., 2002: ASTER Geological Case Histories: Porphyry-Skarn-Epithermal, Iron Oxide Cu-Au and Broken Hill Pb-Zn-Ag. – *Communication in the Workshop “Mapping the Earth with ASTER”*, London.

DRURY, S.A., 1987: Remote sensing of geologic structures in temperate agriculture terrains. – *Geological Magazine* **123**: 113–121.

EGSMA, 1994: Egyptian Geological Survey and Mining Authority. – *Geologic map of Sinai, Arab Republic of Egypt*. Sheet No. 1, scale 1:250,000.

EL MASRY, N.N., HASSEN, I.S. & HEGAZI, A.M., 2003: A Newly recognized example of a Late Precambrian subsurface cauldron subsidence intrusion in Southern Sinai: Jabal Laiq ring dyke. – *5th International Conference on the Geology of the Middle East*: 549–558.

EL SHAFEL, M. & KUSKY, T.M., 2003: Structural and tectonic evolution of the Neoproterozoic Feiran–Solaf metamorphic belt, Sinai Peninsula: implication for the closure of Mozambique Ocean. – *Precambrian Research* **123**: 269–293.

EL SHAFEL, M.K., KHAWASIK, S.M. & EL GHAWABY, M.A., 1992: Deformational styles in the tectonites of Wadi Sa'al area, South Sinai. – *3rd Conference Geological Sinai Development*: 1–8, Ismailia, Egypt.

FARINA, P., CATANI, F., COLOMBO, D., FUMAGALLI, A., KUKAVICIC, M., MARKS, F. & MORETTI, S., 2005: Remote sensing: a tool for landslide investiga-

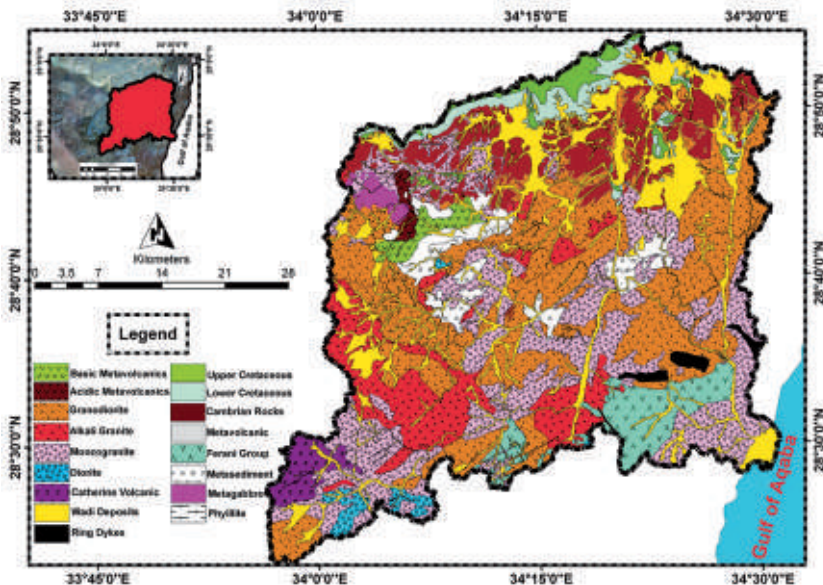


Fig. 14: Final lithological map of Dahab basin area.

- tions at a basin scale. – *Geophysical Research Abstracts* **7**: 10157–10168.
- GAD, S. & KUSKY, T.M., 2007: ASTER spectral ratioing for lithological mapping in the Arabian-Nubian shield, the Neoproterozoic Wadi Kid area, Sinai, Egypt. – *Gondwana Research* **11** (3): 326–335.
- GOMEZ, C., DELACOURT, C., ALLEMAND, P., LEDRU, P. & WACKERLE, R., 2005: Using ASTER remote sensing data set for geological mapping in Namibia. – *Physics and Chemistry of the Earth* **30**: 97–108.
- HASSEN, I.S., IBRAHIM, S.K. & ELEMER, P.M., 2004: Evolution and origin of the metavolcanics at Wadi Saâl area, south Sinai, Egypt. – *Annals Geological Survey Egypt* **27**: 61–78.
- HASSEN, I.S., EL SHAFEL, M.K. & STÜWE, K., 2007: Late Proterozoic crustal evolution in the Arabian-Nubian Shield of Wadi Zaghra tectonites, South Sinai, Egypt. – *Annals Geological Survey Egypt* **V.XXIX**: 77–93.
- HEWSON, R.D., CUDAHY, T.J. & HUNTINGTON, J.F., 2001: Geologic and alteration mapping at Mt Fitton, South Australia, using ASTER satellite-borne data. – *International Geosciences and Remote Sensing Symposium* **2**: 724–726.
- HUME, W.F., 1906: *The Topography and Geology of the Peninsula of Sinai (south-eastern portion)*. – 280 p., Egyptian Survey Department, Cairo.
- HUNT, G.R., 1977: Spectral signatures of particulate minerals in the visible and near infrared. – *Geophysics* **42**: 501–513.
- HUNT, G.R., 1979: Near infrared (1.3–2.4 µm) spectra of alteration minerals – Potential for use in remote sensing. – *Geophysics* **44**: 1974–1986.
- KOBAYASHI, C., ORIHASHI, Y., HIARATA, D., NARANJO, J.A., KOBAYASHI, M. & ANMA, R., 2010: Compositional variations revealed by ASTER image analysis of the Viedma Volcano, southern Andes Volcanic Zone. – *Andean Geology* **37** (2): 433–441.
- KORA, M. & GENEDI, A., 1995: Lithostratigraphy and facies development of Upper Cretaceous carbonates in East Central Sinai, Egypt. – *Facies* **32**: 223–236.
- KNIPLING, E.B., 1970: Physical and physiological basis for the reflectance of visible and near-infrared radiation from vegetation. – *Remote Sensing of Environment* **1**: 155–159.
- MADANI, A. & EMAM, A.A., 2009: SWIR ASTER band ratios for lithological mapping and mineral exploration: A case study from El Hudi area, southeastern desert, Egypt. – *Arabian Journal of Geosciences* **4**: 45–52.
- QARI, M., MADANI, A., MATSAH, M. & HAMIMI, Z., 2008: Utilization of Aster and Landsat data in geologic mapping of basement rocks of Arafat Area, Saudi Arabia. – *Arabian Journal for Science and Engineering* **33** (1C): 99–116.
- REDA, A., KUSKY, T. & GHULAM, A., 2010: Lithological mapping in the Central Eastern Desert of Egypt using ASTER data. – *Journal of African Earth Science* **56**: 75–82.
- ROWAN, L.C. & MARS, J.C., 2003: Lithologic mapping in the Mountain Pass, California area using Advanced Spaceborne Thermal Emission and Reflection Radiometer (ASTER) data. – *Remote Sensing of Environment* **84**: 350–366.
- SAID, R., 1962: *The Geology of Egypt*. – 377 p., Elsevier, Amsterdam.
- SALISBURY, J.W., WALTER, L.S. & VERGO, N., 1987: *Mid-infrared (2.1–25 µm) Spectra of Minerals*. – United States Geological Survey, Open File Report **1**: 87–263, Reston.
- SOLIMAN, F.A. 1986: *Geology of Wadi Sa'al area with special emphasis of metamorphism and tectonics, Central Sinai of Egypt*. – 240 p., Ph.D. thesis, Faculty of Science, Suez Canal University, Ismailia, Egypt.
- WALDHOFF, G., BUBENZER, O., BOLTEN, A., KOPPE, W. & BARETH, G., 2008: Spectral analysis of ASTER, Hyperion and QuickBird data for geomorphological and geological research in Egypt (Dakhla Oasis, Western Desert). – XXI ISPRS Congress, WG VIII/12: 1201–1206, Beijing.
- YAMAGUCHI, Y. & NAITO, C., 2003: Spectral indices for lithologic discrimination and mapping by using the ASTER SWIR bands. – *International Journal of Remote Sensing* **24** (22): 4311–4323.
- ZALATA, A.A., EL METWALLY, A.A., EL AASSY, I.E. & EL SAYED, A.A., 1997: *Evolution and Geochemistry of the Basement rocks of west Dahab area, Southeastern Sinai*. – Third Conference on Geochemistry, Alexandria University: 1–15.

Addresses of the Authors:

ADEL OMRAN and Prof. Dr. VOLKER HOCHSCHILD, Institute of Geoscience, Tübingen University, Rümelinstr. 19–23, D-72070 Tübingen, e-mail: adel-fouad-abdou.omran@student.uni-tuebingen.de, volker.hochschild@uni-tuebingen.de

Prof. Dr. MICHAEL HAHN, Faculty of Geomatics, Computer Science and Mathematics, University of Applied Sciences Stuttgart, Schellingstraße 24, D-70174 Stuttgart, e-mail: michael.hahn@hft-stuttgart.de

Associ. Prof. Dr. AHMED EL-RAYES and Prof. Dr. MOHAMED GERIESH, Faculty of Science, Suez Canal University, University, Ismailia, e-mail: ahmed_elrais@science.suez.edu.eg, helmi_geriesh@yahoo.com

Manuskript eingereicht: März 2012
Angenommen: August 2012